Morphology of electrospun nylon-6 nanofibers as a function of molecular weight and processing parameters

ARTICLE *in* JOURNAL OF APPLIED POLYMER SCIENCE · APRIL 2008

Impact Factor: 1.77 · DOI: 10.1002/app.27655

4 AUTHORS, INCLUDING:

Mehdi Afshari
North Carolina State University
13 PUBLICATIONS **265** CITATIONS

SEE PROFILE

Richard Kotek
North Carolina State University
37 PUBLICATIONS **585** CITATIONS

SEE PROFILE

Russell E Gorga
North Carolina State University
53 PUBLICATIONS **1,779** CITATIONS

SEE PROFILE

Morphology of Electrospun Nylon-6 Nanofibers as a Function of Molecular Weight and Processing Parameters

Satyajeet S. Ojha, Mehdi Afshari, Richard Kotek, Russell E. Gorga

Department of Fiber and Polymer Science, College of Textiles, North Carolina State University, Raleigh, North Carolina 27695-8301

Received 18 May 2007; accepted 16 October 2007
DOI 10.1002/app.27655
Published online 27 December 2007 in Wiley InterScience (www.interscience.wiley.com).

ABSTRACT: In the present study, the morphology and mechanical properties of nylon-6 nanofibers were investigated as a function of molecular weight (30,000, 50,000, and 63,000 g/mol) and electrospinning process conditions (solution concentration, voltage, tip-to-collector distance, and flow rate). Scanning electron micrographs (SEM) of nylon-6 nanofibers showed that the diameter of the electrospun fiber increased with increasing molecular weight and solution concentration. An increase in molecular weight increases the density of chain entanglements (in solution) at the same polymer concentration; hence, the minimum concentration to produce nanofibers was lower for the highest molecular weight nylon-6. The morphology of electrospun fibers also depended on tip-to-collector distance and applied voltage concentration of polymer solution as observed from the SEM images. Trends in fiber diameter and diameter distribution are discussed for each processing variable. Mechanical properties of electrospun nonwoven mats showed an increase in tensile strength and modulus as a function of increasing molecular weight. © 2007 Wiley Periodicals, Inc. J Appl Polym Sci 108: 308–319, 2008

Key words: electrospinning; molecular weight; nanofibers; morphology; mechanical properties

INTRODUCTION

Conventional fiber spinning techniques such as wet spinning, dry spinning, melt spinning, and gel spinning can produce polymer fibers with diameters down to the micrometer range. If the fiber diameter is reduced from micrometers to nanometers, very large surface area to volume ratios can be obtained. These unique qualities make polymer nanofibers an optimal candidate for many important applications.[1] Polymer fibers can be generated from an electrostatically driven jet of a polymer solution or a polymer melt. This process, known as electrospinning, has received a great deal of attention in the last decade because polymer fibers that range from 50 to 500 nm in diameter can be produced.[2–5] Because of the small pore sizes and high surface area inherent in electrospun textiles, these fabrics show promise for applications such as filtration, active surfaces (for biological and/or chemical reactions), drug delivery, and tissue scaffolds.[6–14]

In electrospinning, a high electrical potential (typically between 10 and 20 kV) is applied to a polymer solution in a syringe. Because of the high electric field, the surface tension of the fluid droplet can be overcome and a tapered Taylor cone formed. The fluid jet is then driven toward the grounded collector plate where solid fibers are formed.[1] The jet is the region beyond the tip of the cone where the electrical forces continue to accelerate the fluid and stretch the jet. In this region, the diameter of the jet decreases and the length increases such that a constant amount of mass per unit time passes any point on the axis.[1] Analysis of the flow field in an electrically driven jet showed that the region about the symmetry axis of the jet is free of rotational components and is thus an area of pure extensional flow.[15] The collection region is where the jet is stopped, and the polymer fibers that remain after the solvent evaporates can be collected. The initiation and formation of the jet is a complex and interesting process with many variations.[7] In the electrospinning process, the morphology of the fibers depends on the various parameters such as solution concentration, applied electric field strength, tip-to-collector distance, and fluid flow rate.[16–18] In addition, environmental parameters such as solution temperature, humidity, and air velocity in the electrospinning chamber can affect the process.[9] Although research has provided a fundamental understanding of the process, the fiber morphology as a function of solution properties (concentration, polymer molecular weight) and processing conditions continue to be an area of interest for different systems.

Theoretical analysis in the literature predicted three types of instabilities for an electrically driven jet: axisymmetric Rayleigh instability (irrelevant for electrospinning), electric field-induced axisymmetric

Correspondence to: R. E. Gorga (regorga@ncsu.edu).

TABLE I
Brief Review of Studies Conducted on Different Types of Nylon

Author	Polymer	Solvent	M_w (g/mol)	Focus	Reference
Supaphol	N6	Formic acid, m-chresol, sulphuric acid	17000, 20,000, and 32000	Effects of solvent, polarity of electrode, concentration, and addition of salt (NaCl)	31–33
Gibson	N66	Formic acid	Not reported	Properties of electrospun membranes (moisture transport, air convection, aerosol filtration, tensile strength)	26
Larrondo	N12	-	35000	Modeling of drop formation in terms of a theory Troza	30
Stephen	N6, N12	HFIP	N6: 43,300, N12: 32000	Investigation about chain conformation during electrospinning by Raman spectroscopy	28
Dersch	N6	Formic acid	Not reported	Comparison structure of electrospun and melt spun fibers by x-ray	29
Fong	N6	HFIP, HFIP/dimethyl formamide	20,000	Effects of solvent	27
Bregshoef	N46	Formic acid	Not reported	Transparent composite	8

instability, and whipping instability.[19–21] Bead formation results from axisymmetric instabilities and flow of the electrospun jet. Specifically, applied voltage, solution surface tension, and conductivity can influence the formation of beaded fibers.[22] For example, poly hydroxybutyrate-*co*-valerate (PHBV) fibers electrospun by Zuo et al.[22] showed that higher applied voltage favor formation of smooth fibers and beads are likely to be formed at high feed rate. High surface tension promotes the formation of PHBV electrospun fibers with beads, whereas increased conductivity favors uniform smooth fibers.

Nylon has been widely used as an important engineering plastic because of its good mechanical properties. Nylon fibers have been produced by traditional methods such as melt, wet, and dry spinning. These fibers are available in staple, tow, monofilament and multifilament form.[23] Fiber diameters produced by these methods range from 10 to 500 μm.[24] Therefore producing submicron nylon filaments are of industrial interest.

Researchers have looked at electrospun nylon mats for gas transport and barrier layers,[25,26] changes in crystallinity,[27–29] jet formation from the melt,[30] and mechanical properties as layers in epoxy composites.[8] Specifically, Supaphol and coworkers[31–33] studied the effects of electrode polarity and processing parameters on morphological appearance and size of the as-spun nylon-6 fibers at molecular weight range 17,000–32,000 g/mol. An increase in the temperature of the spinning solutions decreased the size of the as-spun fibers. Addition and increasing content of NaCl caused the conductivity of the spinning solutions to increase which in turn, caused the sizes of the as-spun fibers to increase. Fibers obtained from nylon-6 of higher molecular weights appeared to be larger in diameter. The maximum molecular weight they used was 32,000 g/mol with varying concentration (10–46% w/v). An increase in the temperature of the solution during electrospinning resulted in a decrease in the fiber diameters. Increasing solution viscosity resulted in a reduced number of beads and increased fiber diameters. Diameters of fibers obtained under the negative electrode polarity were larger than those obtained under the positive electrode polarity. Table I summarizes the research done on the electrospinning of different nylon systems.

Therefore, the objectives of this work are to (a) determine the interaction between molecular weight, solution entanglements of the polymer, and processing condition on morphology and mechanical properties of the electrospun mats and (b) clarify which parameter (entanglement density (viscosity) or surface tension) has a more dominant effect on jet stability of the electrospinning process at significantly high molecular weights. In addition, we attempt to produce higher molecular weight nylon-6 (up to 63,000 g/mol) than what has been previously reported[31] in order to demonstrate electrospinning feasibility for nylon-6 with molecular weights of interest for industrial applications.

EXPERIMENTAL

Material

Three molecular weights of nylon-6 were investigated (high (63,000 g/mol), medium (50,000 g/mol) and low (30,000g/mol) molecular weight (ULTRAMID BS700, BS3301, and B4001) from BASF). The viscosity averaged molecular weight was calculated from the Mark-Houwink eq. (1).

$$[\eta] = KM_w^a \quad (1)$$

The constants K and a values used for the nylon-6/formic acid system at 25°C were 22.6×10^{-5} dL/g

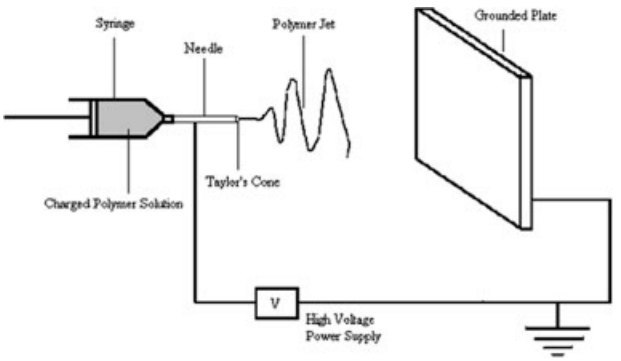

Figure 1 Typical electrospinning setup.

and 0.82, respectively.[34] The viscometric measurements were conducted at 25°C by using an Ubbelohde viscometer. The limiting viscosity number was determined from eq. (2).

$$[\eta] = \frac{2}{C}(\eta_{rel}{}^{1/2} - 1) \quad (2)$$

Here, C is polymer concentration, $[\eta]$ is intrinsic viscosity and η_{rel} is relative viscosity. Two polymer solution concentrations 10 and 15 wt % prepared by dissolving nylon-6 in Formic acid (Merck).

Electrospinning

For electrospinning of nylon-6, a variable high-voltage power supply (Glassman high voltage model FC60R2 with positive polarity) was used to apply voltages of +10, +15, and +20 kV to the horizontally oriented syringe tip. The polymer solution was place in a 10-mL syringe to which a capillary tip of 0.4 mm inner diameter was attached. The positive electrode of the high voltage power supply is connected to the capillary tip. The grounded electrode was connected to a metallic collector wrapped with aluminum foil as shown in Figure 1.

Table II shows sample code and processing parameters of samples. The samples code can be identified as follows:

1. Molecular weight LMW, MMW, and HMW refers to low, medium and high molecular weight nylon-6, respectively.
2. Concentration C_1 and C_2 refers to 10 and 15 wt %, respectively.
3. Voltage V_1, V_2, and V_3 refers to 10, 15, and 20 kV, respectively.
4. Distance from tip to collector D_1, D_2, and D_3 refers to 10, 15, and 20 cm, respectively.
5. Feed rate F_1, F_2, and F_3 refers to 15, 50, and 100 μL/min, respectively.

For example, $LMWC_1V_2F_1D_2$ refers to nanofibers produced from low molecular weight nylon-6 having 10 wt % concentration, at 15 kV voltage, 15 μL/min feed rate, and 15-cm distance.

Morphology

The morphology of the electrospun nylon-6 webs was observed by scanning electron microscopy

TABLE II
Sample Codes and Processing Parameters Used in the Experimental Study

Sample Code	Molecular Weight (g/mol)	Concentration (wt %)	Voltage (kV)	Feed rate (μL/min)	Distance (cm)
$LMWC_1V_2F_1D_2$	30000	10	15	15	15
$MMWC_1V_2F_1D_2$	50000	10	15	15	15
$HMWC_1V_2F_1D_2$	63000	10	15	15	15
$LMWC_2V_2F_1D_2$	30000	15	15	15	15
$MMWC_2V_2F_1D_2$	50000	15	15	15	15
$HMWC_2V_2F_1D_2$	63000	15	15	15	15
$LMWC_2V_1F_1D_2$	30000	15	10	15	15
$LMWC_2V_3F_1D_2$	30000	15	20	15	15
$MMWC_2V_1F_1D_2$	50000	15	10	15	15
$MMWC_2V_3F_1D_2$	50000	15	20	15	15
$HMWC_2V_1F_1D_2$	63000	15	10	15	15
$HMWC_2V_3F_1D_2$	63000	15	20	15	15
$LMWC_2V_2F_1D_1$	30000	15	15	15	10
$LMWC_2V_2F_1D_2$	30000	15	15	15	15
$LMWC_2V_2F_1D_3$	30000	15	15	15	20
$HMWC_2V_2F_1D_3$	63000	15	15	15	20
$MMWC_2V_2F_2D_2$	50000	15	15	50	15
$MMWC_2V_2F_3D_2$	50000	15	15	100	15
$HMWC_2V_2F_2D_2$	63000	15	15	50	15
$HMWC_2V_2F_3D_2$	63000	15	15	100	15
$HMWC_1V_2F_2D_2$	63000	10	15	50	15

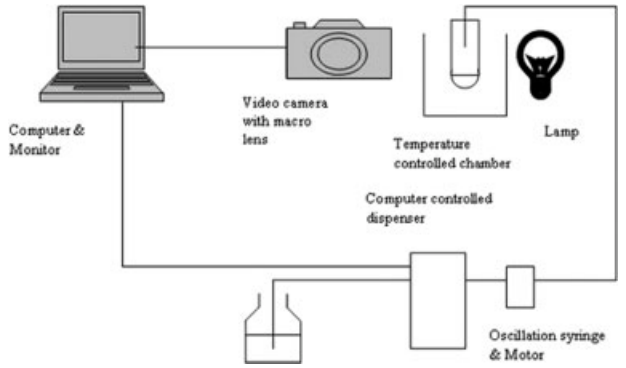

Figure 2 DROP instrument for the measurement of interfacial tension, adapted from Ref. 35.

(SEM) using a JEOL JSM-6400 FE with Energy Dispersive X-ray Spectroscopy (EDS) operating at 5 kV. The electrospun samples were coated (100 Å thickness) with Au/Pd using a K-550X sputter coater to reduce charging. Diameter and void space of the electrospun nylon-6 mats were measured with Image J analysis software.

Interfacial and viscosity measurements

An automated contact angle goniometer (Rame-Hart, Mountain Lakes, NJ) used for data collection and calculations in combination with the DROP image computer program. The capillary drop was formed within an environmental chamber at room temperature, in which standing water increased the relative humidity to minimize evaporation effects. An illustration of the instrument is shown in Figure 2. It consists of a goniometer fitted with a macro lens and autobellows (Olympus) and a CCD video camera. The video frames are captures by a DT3155 frame grabber (Data Translation) in a Pentium 200 PC. The drop control unit is a Microlab M dispenser (Hamilton) and a specially designed oscillation unit consisting of a syringe with an excenter-mounted piston that is motor driven. The dispenser is controlled by the PC. The dispenser and oscillation units are mounted in series with stainless steel pipes that are filled with distilled water. The drops and bubbles are extended from the tip of a small Teflon tube into a quartz cuvette inside a thermostated and water-filled environment chamber with glass windows. The Teflon tube contains an air pocket toward the water in the steel pipe.

The results that are calculated are the surface tension, shape factor (b), radius of curvature (R_0), the drop volume, height and width, the surface area, and the contact angle with the horizontal plane. The surface tension of the monolayers is measured by means of a Wilhelmy plate.[35]

Viscosity was measured using a rheometer (StressTech HR, Rheologica Instruments AB) with rheoExploer V5 operating software using concentric cylinder geometry as the samples were more fluidic. Samples were presheared at 30 Pa for 60 s and all experiments were performed at 25°C.

Mechanical property measurements

An Instron Model 5544 using the Bluehill™ Version 1.00 software was used to measure the tensile properties of the electrospun mats. ASTM D882 method of testing was used for the nonwoven electrospun nylon-6 mats. The gauge length of the mats was 3 cm, and average thickness was 0.14 mm. Tensile properties of electrospun web were measured with 10 mm/min strain rate. Void volume fraction was calculated using Image J analyzer. SEM images were scanned and different layers of nanofibers were made distinct using a gray scale. The void area (proportional to volume) was calculated as area of single nanofiber layer subtracted from total area in that plane.

RESULTS AND DISCUSSION

Effect of molecular weight and concentration on surface tension and viscosity

It is well known that the morphology of electrospun fibers depends on the processing parameters and environmental conditions such as temperature and humidity.[7,8,17,18] The viscosity, net charge density, and surface tension of solution are key parameters for the formation of the stabilized jets.[22] For low and medium molecular weight nylon-6 (at 10 wt % concentration), the solution viscosity (which can be con-

TABLE III
Surface Tension (mN/m) of Nylon-6 Solutions in Formic Acid at Different Molecular Weight and Concentration

Concentration	LMW (30,000 g/mol)	MMW (50,000 g/mol)	HMW (63,000 g/mol)
10 wt %	40.16 ± 0.04	40.17 ± 0.01	40.19 ± 0.05
15 wt %	40.15 ± 0.03	41.35 ± 0.01	41.63 ± 0.01

TABLE IV
Variation in Viscosity as a Function of Molecular Weight and Concentration

Molecular weight (g/mol)	Concentration	Viscosity (cP)
LMW (30,000)	10 wt %	29.6 ± 0.1
MMW (50,000)	10 wt %	37.3 ± 0.3
HMW (63,000)	10 wt %	53.1 ± 0.2
LMW (30,000)	15 wt %	129 ± 0.2
MMW (50,000)	15 wt %	140.1 ± 0.2
HMW (63,000)	15 wt %	154 ± 0.4

trolled by the polymer concentration) was too low to make fibers. Surface tension of the low, medium, and high-molecular-weight nylon-6 with two concentrations (10 and 15 wt %) was measured. At 10 wt % concentration, surface tension almost remains constant among high, medium, and low-molecular-weight nylon-6; however, slight difference was noticed at the concentration of 15 wt %. The results of Table III show that with increasing molecular weight and concentration, change in surface tension is insignificant, whereas viscosity increases appreciably as shown in Table IV. Surface tension, therefore, is not as sensitive to changes in molecular weight and concentration of the polymer in solution as the viscosity.

Effect of concentration and molecular weight on morphology of nanofibers

Polymer solutions are essentially non-Newtonian fluids, elongational flow resists the break up of the viscoelastic jet, leading to the formation of long threads of mini jets. As a result, the morphology of the nanofibrous structure depends on the factors that affect viscosity (such as M_w and concentration).

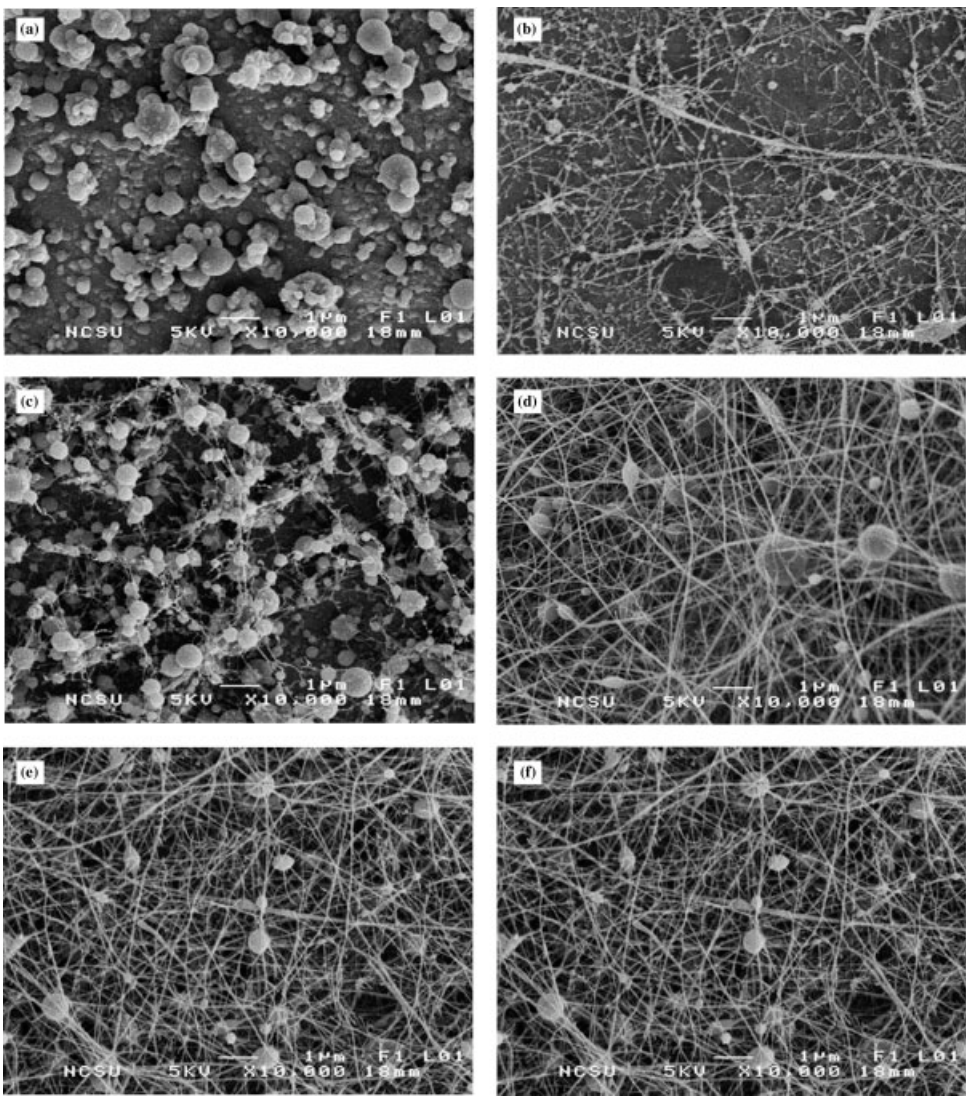

Figure 3 Effect of molecular weight and concentration on morphology of electrospun fibers. Low M_w nylon-6 10 wt % (a) and 15 wt % (b); medium M_w nylon-6 10 wt % (c) and 15 wt % (d); high M_w nylon-6 10 wt % (e), and 15 wt % (f) (All samples at 15kV, 15 μL/min, 15 cm).

TABLE V
Estimation of solution entanglement number for different nylon-6 solutions

Molecular weight (g/mol)	Concentration (wt %)	$(\eta_e)_{sol}$
30,000	10	0.634
30,000	15	0.948
50,000	10	1.05
50,000	15	1.58
63,000	10	1.33
63,000	15	1.99

Hence, polymer concentration and molecular weight have tremendous effect on the viscoelastic jets of nanofibers.[36] Assessment of the SEM of the three nylon-6 molecular weights showed the effect of concentration on the nanofiber morphology as shown in Figure 3. At 10 wt % [Fig. 3(a,c,e)], the morphology changes from beads, to beads on strings, to well-formed nanofibers with a small concentration of beads as the molecular weight increases. At 15 wt % [Fig. 3(b,d,f)], nanofibers are formed with all three molecular weights. However, the LMW sample showed inhomogeneous fiber morphology with beads, the MMW sample showed relatively homogeneous fiber formation with a low concentration of beads, and the HMW sample showed homogeneous fiber formation with almost no beads. A similar trend, at each molecular weight, is also seen for the concentration of polymer in solution. Therefore, as the concentration and molecular weight increases, the concentration of beads decreases. This is due to the increased degree of chain entanglement, which is necessary to form continuous fibers. In addition, a reduction in average bead size was also seen. For example, the average bead size reduced from 434 to 129 nm and the number of beads reduced from $0.465/\mu m^2$ to $0.09/\mu m^2$ in the case of high molecular weight nylon-6 at 10 and 15 wt %, respectively.

A study of the role of chain entanglements in solution during electrospinning has been done by Shenoy et al.,[37] and the expression that relates entanglement density in solution to the molecular properties is given in eq. (3).

$$(\eta_e)_{sol} = \varphi_p M_w / M_e \quad (3)$$

Here, $(\eta_e)_{sol}$ is the solution entanglement number (or density), ϕ_p is volume fraction of polymer in solution, M_w is weight average molecular weight of polymer, and M_e is entanglement molecular weight of polymer (taken to be 5000 g/mol for nylon-6[38]). Based on above equation, $(\eta_e)_{sol}$ was calculated for all three molecular weights and is shown in Table V. We observe that as the value of $(\eta_e)_{sol}$ approaches 2, uniform nanofiber formation is seen with minimal beading (comparing $(\eta_e)_{sol}$ to the SEM images in Fig. 3). As Shenoy points out,[37] as $(\eta_e)_{sol}$ increases, fiber formation (instead of bead formation) becomes more probable until you reach an optimal value where homogeneous nanofibers (without beading) are formed.

Figure 4 shows the diameter distribution for MMW and HMW nylon-6 samples (at 15 wt %, 15 kV, 15 cm, and 15 μL/min). As is shown, the diameter increases with increasing molecular weight from 78 nm for the MMW sample to 107 nm for the HMW sample, but the diameter distribution narrows. The increase in diameter with molecular weight is attributed to decreased mobility of the polymer chains. Therefore, at higher molecular weights less extension (and therefore less densification) is expected and the overall fiber diameter increases. Skivkumar and coworkers[39] use the longest relaxation time (λ) of the molecules in solution from the Rouse model [Eq. (4)] to justify the increase in diameter with molecular weight for poly vinyl alcohol.

$$\lambda \approx 6\,\eta_s[\eta]M_w/\pi^2 RT \quad (4)$$

In Eq. (4), η_s is the solvent viscosity, $[\eta]$ is the intrinsic viscosity, R is the gas constant and T is the temperature. An increase in molecular weight increases the relaxation time of the polymer. The relaxation times for LMW, MMW, and HMW nylon-6 [from Eq. (4)] were calculated as 1.65×10^{-2}, 3.35×10^{-2}, and 5.48×10^{-2} s, respectively. Using this rationale, an increase in molecular weight results in decreased relaxation of polymer chains and as a consequence, the elongational flow is reduced and nanofibers with larger diameters are obtained.

Effect of voltage on morphology of nanofibers

Voltage has a strong effect on morphology of nylon-6 nanofibers as shown by the SEM micrographs in Figure 5. Electrospinning was performed at three

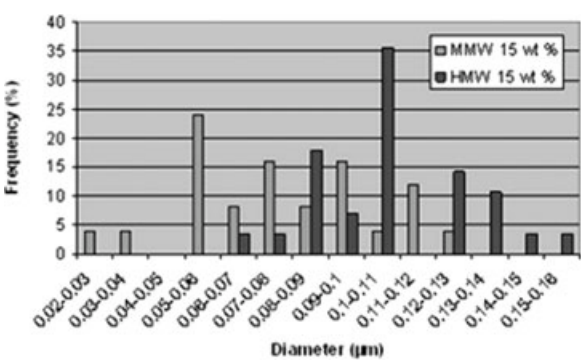

Figure 4 Effect of molecular weight (MMW and HMW) on diameter distribution (15 wt %, 15 KV, 15 cm, and 15 μL/min).

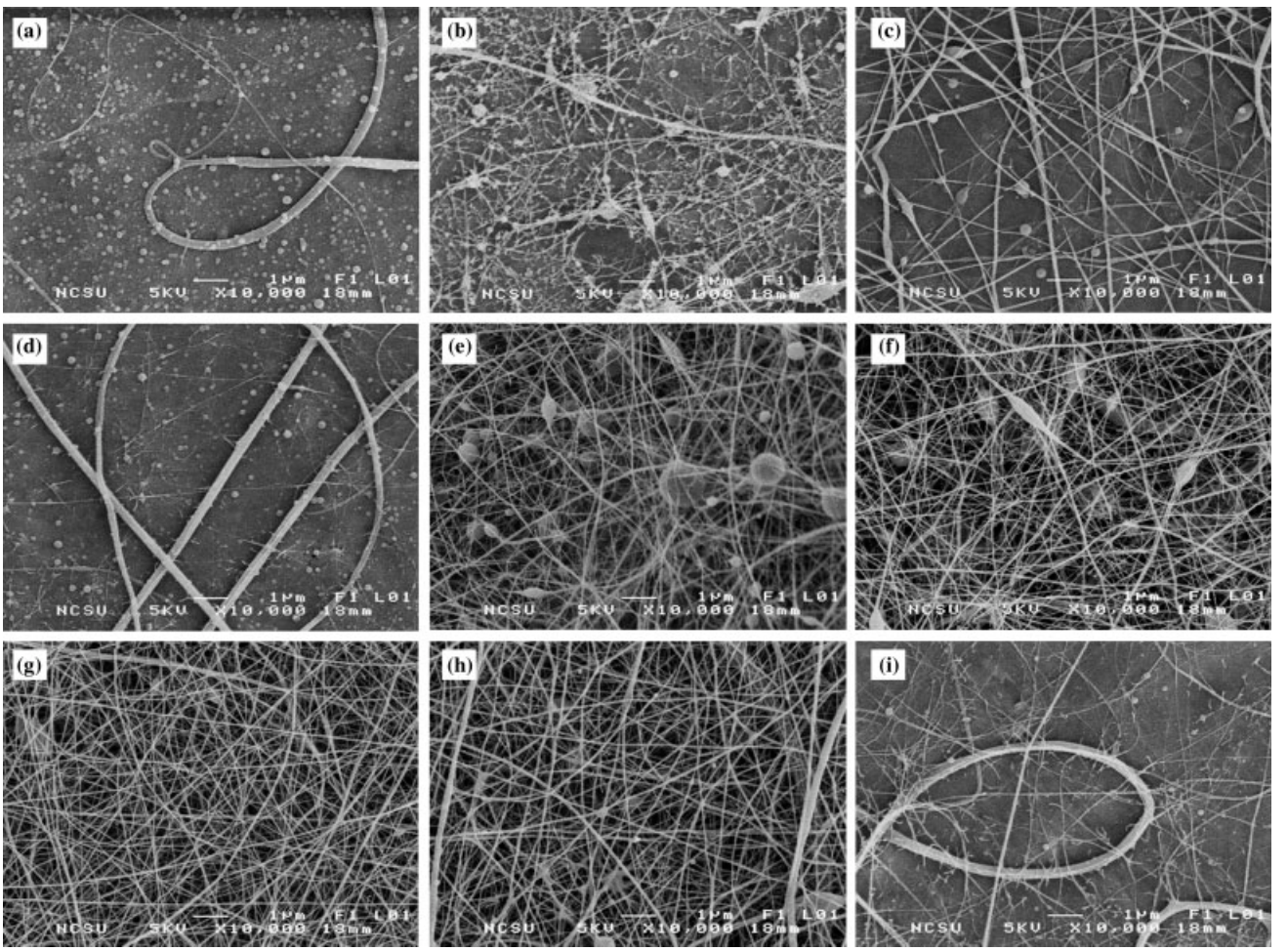

Figure 5 Effect of voltage on morphology for (a, b, c). Low M_w nylon-6 at 10, 15, 20 kV; (d, e, f) medium M_w nylon-6 at 10, 15, 20 kV; (g, h, i) high M_w nylon-6 at 10, 15, 20 kV (All samples at 15 wt %, 15 μL/min, 15 cm).

voltages (10, 15, and 20 kV), and all other parameters (concentration, distance and feed rate) were kept constant at 15 wt %, 15 cm, and 15 μL/min, respectively.

As shown in Figure 5 for the low and medium molecular weight nylon samples, as the voltage was increased from 10 to 20 kV there is a dramatic change in the overall fiber morphology. For both molecular weights, the samples produced at 10 kV are rope-like with a very low concentration of fibers. At 15 kV, the typical nanofiber morphology is seen (with the presence of some beads). With the HMW nylon-6, the reverse trend is seen. At 10 and 15 kV, the typical nanofiber morphology is observed but at 20 kV the rope-like fibers are present (with very few nanofibers). It is clear that there is an optimum voltage condition characteristic of the polymer molecular weight, which maximizes the whipping instability to form thin fibers. This effect is also similar to that for very high feed rates (as discussed later). Although fibers were formed from the whole range of molecular weights and voltages produced, the HMW sam-

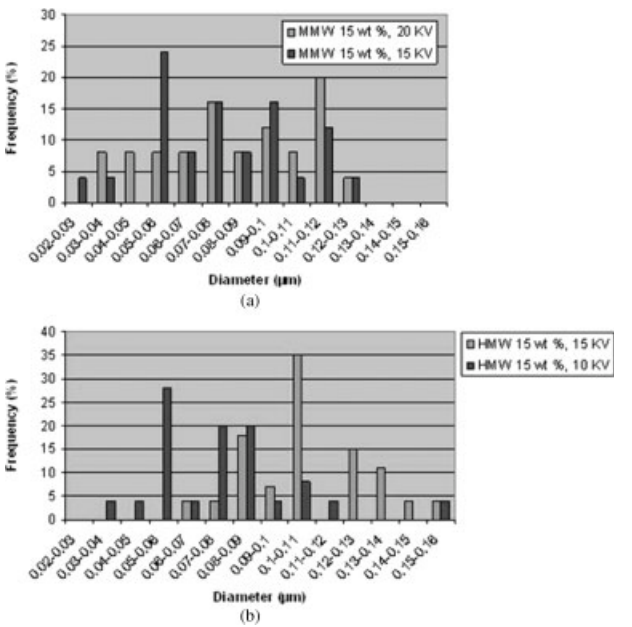

Figure 6 (a, b): Diameter distribution as a function of voltage for medium M_w (a) and high M_w (b) nylon-6 (15 wt %, 15 cm, 15 μL/min).

ples (at 10 and 15 kV) were without beads and more uniform than those at the lower molecular weights.

Excluding the rope-like samples, Figure 6 shows the diameter distributions for the MMW and HMW samples as a function of voltage. Average diameter of nanofiber for the MMW slightly increased from 78 nm at 15 kV to 83 nm at 20 kV. For the HMW, the average diameter slightly increased from 77 nm at 10 kV to 107 nm at 15 kV. The rationale behind this observation is that an increase in voltage drives the charged jet to emerge from tip through Taylor's cone rapidly due to higher electrostatic forces, so more solution is ejected, resulting in an increase in fiber diameter and a broadening of the diameter distribution. These results agree with work carried out by Zhang and coworkers.[40]

Effect of distance on morphology of nanofibers

The distance between the tip of the capillary and the grounded plate can have a significant impact on morphology of electrospun nanofibers. Three different distances were chosen 10, 15, and 20 cm between the tip of the needle and the grounded plate (tip-to-collector distance). For a particular molecular weight, other parameters such as concentration, voltage and feed rate were kept constant at 15 wt %, 15 kV and 15 μL/min, respectively.

As the distance between the tip and grounded plate increased, more uniform and beadless nanofiber were obtained in all nylon-6 samples. Figure 7(a–c) shows the trend observed for the LMW samples. We see that as the distance increased from 10 to 20 cm, a progressive reduction in bead occurrence

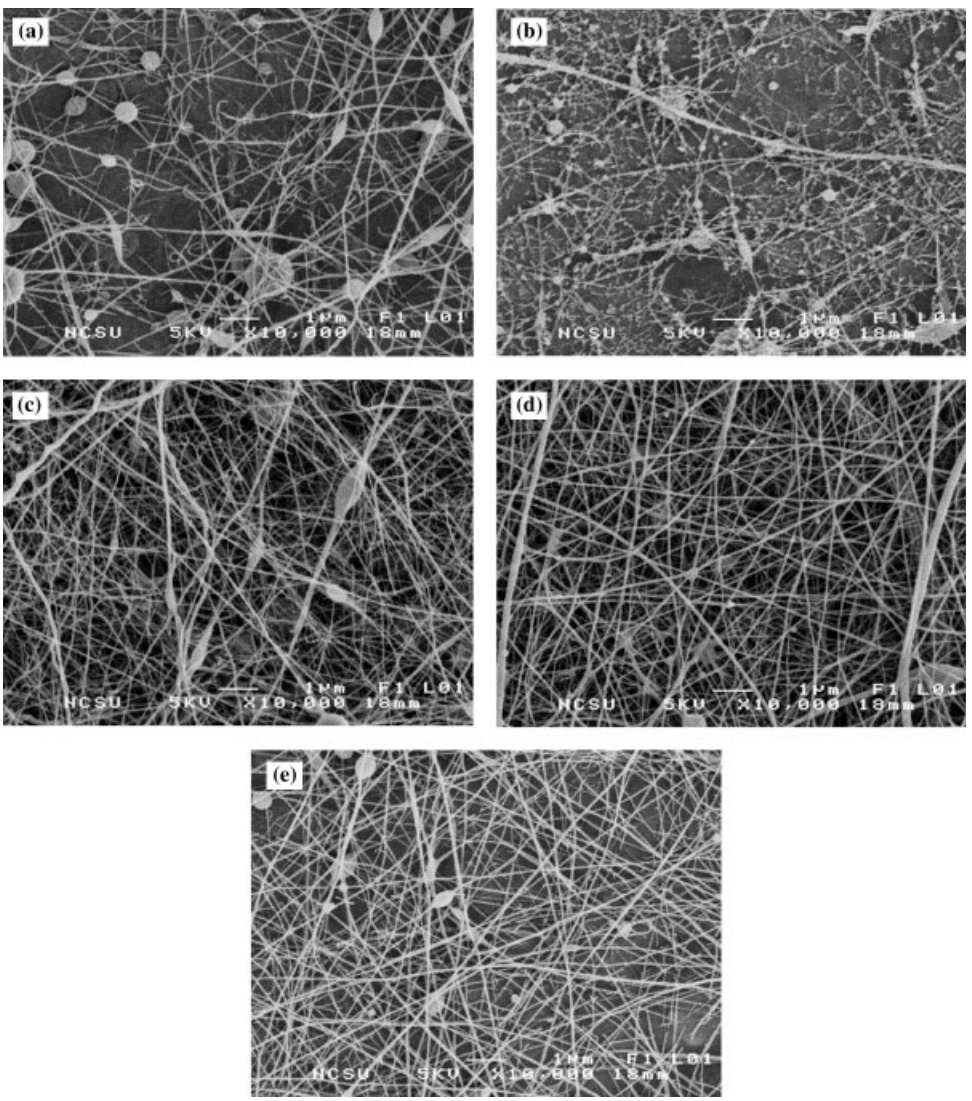

Figure 7 Effect of distance on nanofiber morphology for (a, b, c). Low M_w nylon-6 at distance 10, 15, and 20 cm. (d, e) High M_w nylon-6 at distance 15 and 20 cm (All samples at 15 wt %, 15 KV, 15 μL/min).

and an increase in fiber concentration is observed. Identical trends were observed in the case of medium and high molecular weight samples (MMW are samples omitted since the trend in morphology was so similar to that for LMW samples). Figure 7(d,e) shows that the HMW samples showed more consistent nanofibers as compared to the LMW samples. We observed that there is a difference in the morphology of the nanofibers from two samples at similar conditions. The low molecular weight samples are less uniform with more beads as compared to high molecular weight nylon-6 as predicted by Shenoy et al.[37] based on entanglement concentration.

Figure 8(a) quantitatively shows that in case of low molecular weight nylon-6 that as distance increases the diameter of nanofibers decreases. The average diameter decreased from 78 to 65 nm and the diameter distribution became narrower. We observe the same trend for the high molecular weight fibers [as shown in Fig. 8(b)]. The average diameter decreased from 107 to 96 nm, and the diameter distribution becomes narrower as the tip-to-collector distance is increased. An increase in distance provides more time and distance for the whipping instability, resulting in finer nanofibers and a more uniform diameter distribution.

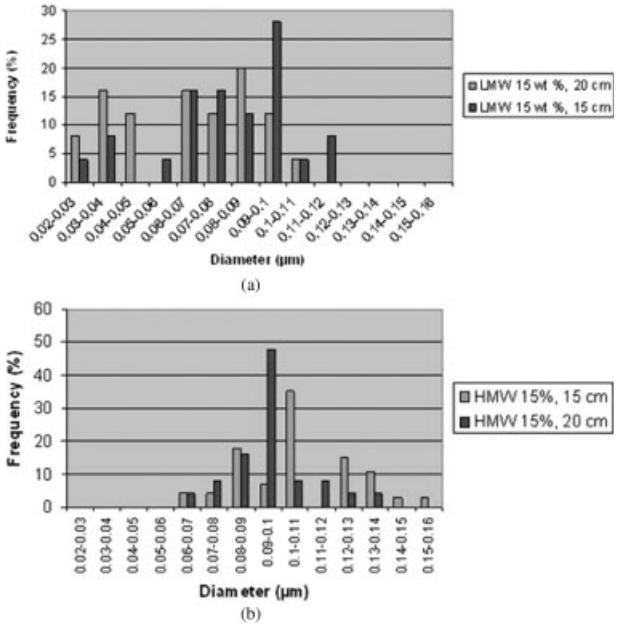

Figure 8 Diameter distribution as a function of collector distance for (a) low and (b) high-molecular-weight samples (15 wt %, 15 kV, and 15 µL/min).

Effect of feed rate on morphology of nanofibers

Three feed rates (15, 50 and 100 µL/min) were chosen to determine the effect of mass throughput on fiber morphology. Other parameters such as concentration, voltage, and distance were kept constant at 15 wt %, 15 kV, and 15 cm, respectively. The general trend depicted an increase and then decrease in fiber forming tendency as the feed rate was increased.

For the MMW samples, nanofibers with typical beads on string structure were observed at 15 µL/min. When the feed rate was increased to 50 µL/min, the frequency of beads decreased and more slender nanofibers were formed. At 100 µL/min, no nanofibers were formed, instead the rope-like structure was seen [Fig. 9(c)]. For the HMW samples at 15 wt % [Fig. 9(d–f)], a different trend was observed, at the lowest feed rate, homogeneous nanofibers were formed. As the feed rate increased, there was a higher concentration of beads (although the fiber diameter decreased). The 10 wt % concentration of high molecular weight nylon-6 was also evaluated [Fig. 9(g,h)]. At 10 wt % a similar trend was seen; however, the concentration and size of the beads was increased. As the feed rate increases, more polymer is available at the needle tip to be electrospun which at some point will exceed the rate of removal at a fixed electric field and nonuniform drawing takes place resulting in beaded nanofibers.

The diameter distribution in Figure 10 shows that the average diameter increased from 107 to 119 nm as the feed rate was increased from 15 to100 µL/min in the case of high molecular weight (15 wt %) nylon-6. In the case of MMW (15%) as shown in Figure 10(b), the average diameter increased from 78 to 81 nm as the feed rate increased from 15 to 50 µL/min, and at 100 µL/min no nanofibers formed. For both high and medium molecular weight samples, the diameter distribution of electrospun fibers became broader with increasing feed rate.

Mechanical testing of nanofibrous mats

It is known that as the molecular weight of a polymer increases, mechanical properties in the bulk also increase due to increased number of chain entanglements. However, it is unclear what the effect of M_w has on the mechanical properties of the fibrous mat would be, since the mechanical properties are dependent on both fiber properties as well as the bond strength at the fiber–fiber junctions. As M_w increases we expect fiber strength/modulus to increase, however we are unsure of the effect M_w will have on the strength of the fiber–fiber weld points, or in other words, how the M_w affects the bonding between fibers in the mats, which is an interesting topic for future research (we would expect the interdiffusion to decrease as M_w increases, but are unsure of how that will affect the weld strength).

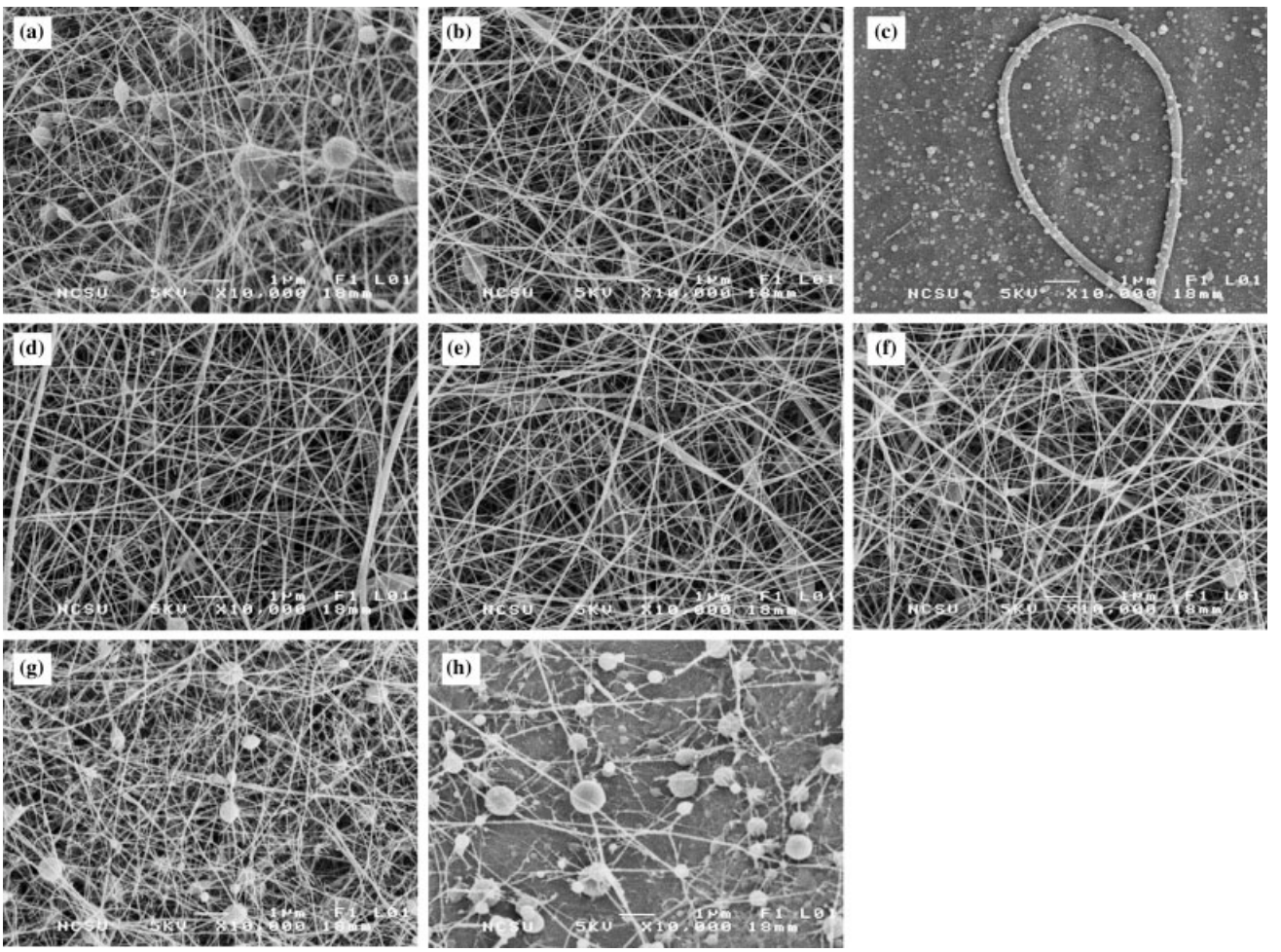

Figure 9 Effect of feed rate on morphology for (a, b, c) medium M_w 15 wt % nylon-6 at 15, 50, 100 μL/min; (d, e, f) high M_w 15 wt % nylon-6 at 15, 50, 100 μL/min; (g, h) high M_w 10 wt % nylon-6 at 15 and 50 μL/min (All samples at 15 wt%, 15 KV, 15 cm).

The mechanical test results (Table VI) showed that as the molecular weight increased, modulus and tensile strength of the nonwoven electrospun nanofibrous mats increased. The increase in mechanical properties between the LMW and MMW samples is quite pronounced, however there is no statistical difference in the mechanical properties between the MMW and HMW samples. This is not unexpected since the molecular weight between LMW and MMW nearly doubles (and goes through a critical M_w transition ($\sim$8 M_c) above which the mechanical properties remain constant with respect to M_w). The tests were performed on nanofibrous electrospun mats having identical processing conditions: concentration (15 wt %), feed rate (15 μL/min), tip-to-collector distance (15 cm), and electric field (15 kV). In addition, each of the experiments was timed to keep the thickness of mats relatively uniform (0.1 mm). Five samples of each molecular weight were tested for statistical purposes. These results account for the porosity of the mats where the void volume fraction was measured using Image J software. The

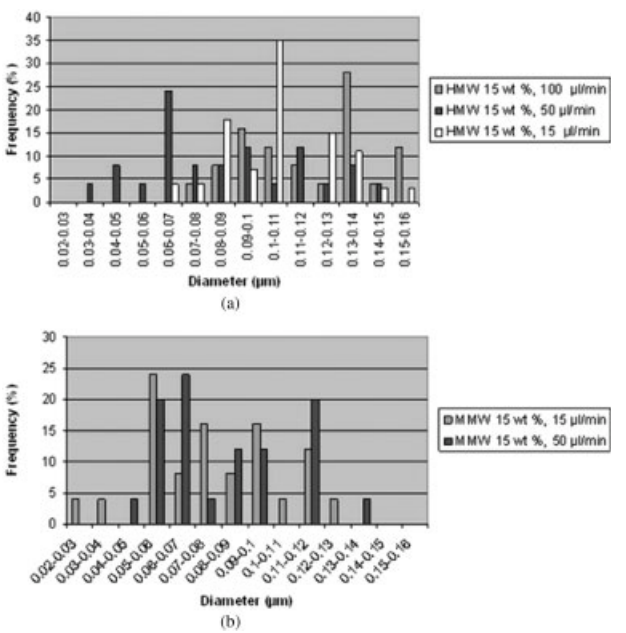

Figure 10 (a, b) Effect of Feed rate on diameter distribution on high M_w (a) and medium M_w (b) shows a drop off in overall diameter size (15 wt %, 15 kV, and 15 cm).

TABLE VI
Tensile Properties of Electrospun Nylon-6 Web

Electrospun web	Tensile strength (MPa)	Elongation at break (%)	Modulus (MPa)
HMW	52 ± 5	16.6 ± 2.5	333 ± 39
MMW	46 ± 2	18.7 ± 0.8	332 ± 45
LMW	21 ± 2	9.3 ± 1.7	231 ± 15

void volume fraction for high, medium and low molecular weight nylon-6 samples was calculated as 85, 87, and 86%, respectively. Table VI shows that Young's modulus increased almost 50% as a function of increasing molecular weight. Tensile strength more than doubled as M_w increased. Therefore the increase in M_w did not have an adverse effect on the molecular interdiffusion and the resulting strength of the fiber–fiber junctions (within the M_w range studied).

CONCLUSION

In the present endeavor, the electrospinning technique was used to produce nanoscale fibers of nylon-6. The core objective of this study was to fabricate nanofibers of high molecular weight of nylon-6 to understand the effect molecular weight has on morphology and mechanical properties of electrospun fibrous mats. Variation in surface tension was shown to be insignificant as a function of changes in molecular weight and concentration of the polymer. Not surprisingly however, the viscosity was strongly influenced by changes in molecular weight and concentration. Molecular weight and concentration significantly affect the morphology of the nanofibers.

Changes in voltage have a strong effect on the morphology on nanofibers. With an increase in voltage, more fibers are formed with less beads and larger diameters. For high-molecular-weight nylon-6, it was possible to manufacture nanofibers at lower voltages (as compared with low and medium-molecular-weight nylon-6). With an increase in tip-to-collector distance (thereby increasing the time of flight of nanofibers), a reduction in diameter size is observed (as well as the diameter distribution). The diameter of electrospun nanofibers increased with an increase in feed rate. Favorable feed rate to produce nanofibers was higher in case of low molecular weight and lower in case of high molecular weight nylon-6. Mechanical properties showed that tensile strength as well as modulus increase as molecular weight is increased with no apparent negative effects on bonding at the fiber–fiber junctions.

We gratefully acknowledge Professor Wendy Krause for useful discussions and Dr. Dale Batchelor for kindly helping and providing us SEM micrographs. We are thankful to Dr. Brian E. Farkas and Paige Luck for helping us in Surface Tension measurements and Jamal Irving for contributing efforts in the laboratory.

References

1. Huang-Zhang, Y. Z.; Kotaki, M.; Ramakrishna, S. Compos Sci Technol 2003, 63, 2223.
2. Pedicini, A.; Farris, R. J. J Polym Sci B: Polym Phys 2004, 42, 752.
3. Deitze, J. M.; Kosik, W.; McKnight, S. H.; Beak-Tan, N. C.; Desimone, J. M.; Crette, S. Polymer 2002, 43, 1025.
4. Ding, B.; Kim, H. Y.; Lee, S. C.; Shao, C. L.; Lee, D. R.; Park, S. J.; Kwag, G. B.; Choi, K. J. J Polym Sci Part B: Polym Phys 2002, 40, 1261.
5. Dai, H.; Gong, J.; Kim, H. Y.; Lee, D. R. Nanotechnology 2002, 13, 674.
6. Deitzel, J. M.; Kleinmeyer, J.; Harris, D.; Beck-Tan, N. C. Polymer 2001, 42, 261.
7. Reneker, D. H.; Chun, I. Nanotechnology 1997, 7, 216.
8. Bergshoef, M. M.; Vancso, G. J. Adv Mater 1999, 11, 362.
9. Doshi, J.; Renker, D. H. J Electrostat 1995, 35, 151.
10. Gibson, P. W.; Schreuder-Gibson, H. L.; Riven, D. AIChE J 1999, 45, 190.
11. Fong, H., Renker, D. H. In Electrospinning and Formation of Nanofibers; Salem, D. R.; Sussman, M. V., Eds.; Hanser: Munich, 2001; Chapter 6.
12. Hou, H.; Jun, Z.; Reuning, A.; Schaper, A.; Wendorff, J. H.; Greiner, A. Macromolecules 2002, 35, 2429.
13. Kenawy, E. R.; Bowlin, G. L.; Mansfield, K.; Layman, J.; Simpson, D. G.; Sanders, E. H. J Controlled Release 2002, 81, 57.
14. Scopelianos, A. G. U.S. Pat. 5,522,879 (1996).
15. Larrondo, L.; Manley, R. J Polym Sci Part B: Polym Phys 1981, 19, 921.
16. Fong, H.; Chun, I.; Renker, D. H. Polymer 1999, 40, 4585.
17. Bognitzki, M.; Czado, W.; Frese, T.; Schaper, A.; Hellwig, M.; Steinhart, M.; et al. Adv Mater 2001, 13, 70.
18. Lee, K. H.; Kim, Y. H.; La, Y. M.; Lee, D. R.; Sung, N. H. J Polym Sci Part B: Polym Phys 2002, 40, 2259.
19. Hohman, M. M.; Shin, M.; Rutledge, G.; Brenner, M. P. Phys Fluids 2001, 13, 2201.
20. Shin, Y. M.; Hohman, M. M.; Brenner, M. P.; Rutledge, G. C. Appl Phys Lett 2001, 78, 1149.
21. Shin, Y. M.; Hohman, M. M.; Brenner, M. P.; Rutledge, G. C. Polymer 2001, 42, 9955.
22. Zuo, W.; Zhu, M.; Yang, W.; Yu, H.; Chen, Y.; Zhang, Y. Polym Eng Sci 2005, 45, 704.
23. Zimmerman, J.; Mark, H. F.; Bikales, N. M. In Encyclopedia of Polymer Science and Engineering; Wiley: New York, 1988; Vol. 6, p 802.
24. Ziabicki, A. Fundamentals of Fiber Formation: The Science of Fiber Spinning and Drawing; Wiley: New York, 1976.
25. Ryu, Y. J.; Kim, H. Y.; Lee, K. H.; Park, H. C.; Lee, D. R. Eur Polym J 2003, 39, 1883.
26. Schreuder-Gibson, H. L., Gibson, P., Senecal, K., Sennett, M., Walker, J., Yeomans, W. J Adv Mate 2002, 34, 44.
27. Fong, H.; Liu, W.; Wang, C.; Vaia, R. A. Polymer 2002, 43, 775.
28. Stephen, J. S.; Chase, D. B.; Rabolt, J. F. Macromolecules 2004, 37, 877.
29. Dersch, R.; Liu, T.; Schaper, A. K.; Greiner, A.; Wendorff, J. H. J Polym Sci Part A: Polym Chem 2003, 41, 545.

30. Larrondo, L.; Manley, R. J Polym Sci Part B: Polym Phys 1981, 19, 933.
31. Supaphol, P.; Upnylontham, C. M.; Nithitanakul, M. J Polym Sci Part B: Polym Phys 2005, 43, 3699.
32. Uppatham, C. M.; Nithitanakul, M.; Supaphol, P. Macromol Chem Phys 2004, 205, 2327.
33. Supaphol, P.; Uppatham, C. M.; Nithitanakul, M. Macromol Mater Eng 2005, 290, 933.
34. Bandrup, J.; Immergut, E. H. Polymer Handbook; Wiley: New York, 1975.
35. Myrvold, R.; Hansen, F. K. J Colloid Interface Sci 1998, 207, 97.
36. Mun, R. P.; Byars, J. A.; Boger, D. V. J Non-Newtonian Fluid Mechanics 1998, 74, 285.
37. Shenoy, S. L.; Bates, W. D.; Frisch, H. L.; Wnek, G. E. Polymer 2005, 46, 3372.
38. Aharoni, S. M. Macromolecules 1983, 16, 1722.
39. Koski, A.; Yim, K.; Shivkumar, S. Mater Lett 2004, 58, 493.
40. Zhang, C.; Yuan, X.; Wu, L.; Han, Y.; Sheng, J. Eur Polym J 2005, 41, 423.